Novel aluminium/polyvinylidene fluoride metastable intermolecular composite film prepared by solution casting method

Pengfei He, Yajun Wang ✉, Shihui Li, Yi Wan

State Key Laboratory of Explosion Science and Technology, Beijing Institute of Technology, Beijing 100081, People's Republic of China
✉ *E-mail: yajunwang@bit.edu.cn*

Published in Micro & Nano Letters; Received on 16th April 2020; Revised on 16th June 2020; Accepted on 30th June 2020

One challenge in the application of traditional metastable intermolecular composite (MIC) material is that MIC particles are not compatible with micro-electro-mechanical system. In the authors' work, a solution casting method was employed to prepare aluminium/polyvinylidene fluoride (Al/PVDF) MIC films. The morphological, structural and compositional information of the samples were characterised by scanning electron microscopy, X-ray diffraction, energy dispersive spectroscopy and Fourier transform infrared spectroscopy. The energy-release characteristics of Al/PVDF films were studied by thermogravimetric analysis and differential scanning calorimetry. The results show that heat output and mass loss increased as the thickness of MIC films reduced. The maximum heat release of the main exothermic peak was 1032 J/g. The kinetics process could be divided into three stages with apparent activation energy calculated by Kissinger and Starink methods of 128.86, 164.69 and 153.16 kJ/mol, respectively.

1. Introduction: Metastable intermolecular composite (MIC) is a mixture of nano-scale fuel and oxidant with high energy, high activity and low sensitivity, pioneered by Lawrence Livermore National Laboratory in 1995 [1]. MIC obviously affects the performance of initiation, ignition and specific impulse. It can improve the performance of sensitivity, stability, energy release speed and mechanical properties, and has great energy density [2, 3].

In the traditional thermite reaction, aluminium powder is the most commonly used fuel, and the oxidant is often metal oxide [4–8]. Nano-aluminium (n-Al) has been received much interest due to its low ignition temperature and high burning rate associated with the enhanced specific surface area [9]. The reaction can be summarised in (1), where M_aO_b represents a metal oxide, which will be reduced to a metal (M) in the reaction [10]

$$\frac{2b}{3}\mathrm{Al} + \mathrm{M}_a\mathrm{O}_b \rightarrow \frac{b}{3}\mathrm{Al}_2\mathrm{O}_3 + a\mathrm{M} \quad (1)$$

However, an obvious disadvantage of n-Al powder is the existence of an oxide layer on its surface. The continuously formed oxide layer (Al_2O_3, 2–6 nm) on the outside of the aluminium nanoparticles causes the continuous loss of effective components. At the same time, the oxide layer increases the diffusion resistance of the active aluminium atoms inside the particles during the exothermic reaction, limiting the reaction activity. Therefore, it has certain limitations as a fuel in the MICs system.

In recent years, some researchers have discovered that fluoropolymers can act as oxidisers of MICs, which can have a pre-ignition reaction (PIR) with n-Al. This step can effectively remove the oxide layer on the surface of n-Al core while releasing heat. At present, many researches focus on polytetrafluoroethylene (PTFE) due to its high fluorine content of up to 76 wt% [11]. However, there are relatively few studies on polyvinylidene fluoride (PVDF). In fact, the fluorine content of PVDF is as high as 59.4 wt%, and compared with PTFE, PVDF is more likely to react with n-Al. In addition, PTFE is almost insoluble in any solvent, which limits its scope of application, and PVDF can just make up for this defect. The reaction equation between PVDF and n-Al can be summarised in (2), where CH_2CF_2 represents a unit of PVDF [12, 13]. Another benefit of using fluoropolymer is that it can be used as a passivation layer to prevent the further oxidation of Al core [13]

$$2\mathrm{Al} + 3 - [- \mathrm{CH}_2\mathrm{CF}_2 -]_n - \rightarrow 2\mathrm{AlF}_3 + 6\mathrm{C} + 3\mathrm{H}_2 \quad (2)$$

PVDF has been demonstrated to be both a strong oxidant and an efficient binder [14]. He *et al.* [15] found that n-Al was activated by eliminating Al_2O_3 through the etching reaction between PVDF and Al_2O_3. Guo *et al.* [16] fabricated aluminium/polyvinylidene fluoride (Al/PVDF) MIC film by spin coating method, and demonstrated that the appropriate amount of coupling agent γ-methacryloxypropyl trimethoxy silane (KH-570) can not only improve the dispersibility of n-Al in the film significantly, but also advance the temperature of the reaction between Al_2O_3 shell and fluorine from 372 to 350°C. Wang *et al.* [17] discovered that the reaction speed of Al/PVDF is increased by three times when adding 5 wt% mesoporous SiO_2 (meso-SiO_2). The presence of meso-SiO_2 seems to accelerate the decomposition of PVDF, and the significant increase in hydrogen fluoride (HF) release results in the increased heat release. Ke *et al.* [18] prepared Al/PVDF nano-energetic thin films by vacuum freeze-drying technique to improve the safety of the preparation process of energetic materials. The morphology and composition characterisation confirmed that n-Al was uniformly dispersed in the hydrophobic binder, which made the film have higher waterproof, anti-ageing and anti-corrosion characteristics. Besides vacuum freeze-drying technology, high-temperature operation can also be avoided in the preparation of MIC films by solution casting method, a simple, efficient and low-cost process, thus effectively ensuring the safety of operation [19]. Wang *et al.* [20] compared the mechanical, ignition and combustion properties of three energy-containing films (Al/PVDF, Al/Viton and Al/THV). It was found that Al/PVDF films had the highest tensile stress (~35 MPa) and the fastest burning rate, but the flame temperature (1500 K) was lower than those of the other two films. In addition, compared with the Al/metal oxide MIC system [21], the reaction temperature of Al/PVDF nano-thermite is lower, which can reduce the ignition delay time to a certain extent.

In this work, we use solution casting method to prepare Al/PVDF composite films with three different thicknesses. By now little literature is available on the preparation of energetic composite

films by solution casting method. The prepared films of n-Al in PVDF matrix are smooth and homogeneous. The microscopic structure and composition of the films were characterised by scanning electron microscopy (SEM), energy dispersive spectroscopy (EDS) and X-ray diffraction (XRD). Fourier transform infrared spectroscopy (FTIR) was employed to determine structural information, and the thermal behaviour was studied by thermogravimetric (TG) and differential scanning calorimetry (DSC).

2. Experimental

2.1. Fabrication of Al/PVDF composite film: The stoichiometric reaction of Al and PVDF producing HF, AlF_3 and carbon (in (2)) requires 22% Al and 78% PVDF by weight. In this study, PVDF of 0.2500 g was dissolved in N, N-dimethylformamide (DMF) of 2 ml with magnetic stirring for 30 min. Then 0.0840 g spare Al powder (50 nm) and 1 µl γ-methacryloxypropyl trimethoxy silane (KH-570) were added into above DMF solution with PVDF dissolved in and the mixture was magnetically stirred for half an hour. The composite film was obtained by solution casting method, and the thickness of the film was controlled by a drawing knife. Three different Al/PVDF MIC films with varying thickness of central layer were fabricated and the process is shown in Fig. 1. After that the film was dried in a vacuum oven at 60°C for 6 h to evaporate the solvent completely. Finally, the Al/PVDF MIC film was obtained.

2.2. Characterisation: The surface morphology of the materials was observed by a BACPC S-4800 SEM equipped with EDS. The crystal phase and composition of the samples were measured by XRD (Bruker D8 with Cu Kα radiation) and FTIR (VERTEX80).

TG and DSC analyses were performed on a SDTQ600 simultaneous DSC/TGA analyser (TA instruments) under flowing nitrogen (50 ml/min). In a typical test, 2–5 mg samples were placed into an alumina pan, and heated from room temperature up to 800°C at the rates of 5, 10, 15 and 20 K/min, respectively.

3. Results and discussion: Fig. 2 shows the SEM images of a Al/PVDF film (thickness of 100 µm). The composite films are crack free, smooth and uniform. Nano-aluminium powder is usually easy to agglomerate, but it can be seen from the SEM images that n-Al powders are basically uniformly dispersed in the PVDF film, and there is no serious particle aggregation phenomenon, which proves that n-Al powder has good compatibility with PVDF polymer due to the high mixing degree of domains of n-Al and $–CH_2–CF_2–$ in a gel network during preparation process [22]. However, a little agglomeration still exists, which may be affected by the cast speed of drawing knife. Since PVDF dissolves in DMF to form a viscous liquid, which could perfectly wrap n-Al. In addition, coating a polymer layer to limit oxygen diffusion has been considered an effective way to prevent further oxidation of n-Al [18, 23, 24]. Therefore, PVDF matrix can be expected to provide protection on n-Al.

The EDS mapping (Fig. 3) shows that Al/PVDF film is dense and n-Al particles are evenly dispersed in the PVDF matrix. The spectra on the surface indicate all desired element signals of C, F and Al. The mass fractions of C, F and Al are 46.98, 31.26 and 21.76%, respectively. According to (2), the theoretical mass content of n-Al should be 21.95%, and the actual result is quite close to the theoretical value. Thus, the results demonstrate that the Al/PVDF MIC film preparation by solution casting method is successful.

XRD patterns of pure PVDF, Al, Al/PVDF film and reaction residue are shown in Fig. 4. The characteristic peaks at 18.3°, 19.9° and 26.7° belong to α phase of PVDF and the weak peak at 20.6° is attributed to β phase [25], which shows the semi-crystalline structure of pure PVDF matrix. N-Al particles have strong diffraction peaks at $2\theta = 38.4°$, 44.7°, 65.0°, 78.2° and 82.4°, corresponding to (111), (200), (220), (311) and (222) planes, respectively. Compared with those of pure PVDF and Al, the XRD curve of Al/PVDF film shows no significant change in peak location. However, the intensity of the diffraction peak reduced and PVDF has only one characteristic peak ($2\theta = 19.9°$). This may be due to the destruction of the crystallisation of polymer matrix (PVDF) during the preparation of Al/PVDF. The reaction residue was also analysed by XRD. The strong diffraction peaks at $2\theta = 25.3°$, 42.6°, 51.9° and 58.0°, corresponding to

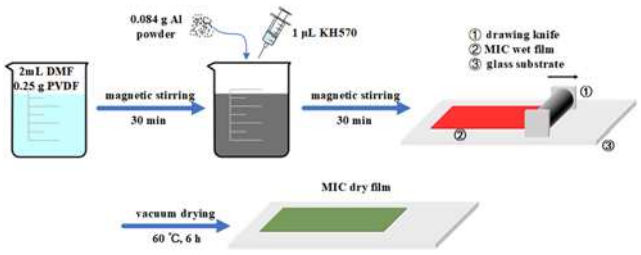

Fig. 1 *Schematic illustration of preparation of Al/PVDF films by solution casting method*

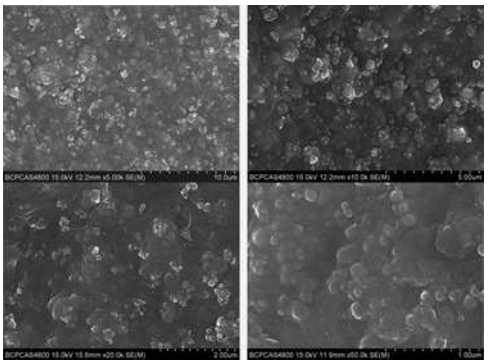

Fig. 2 *SEM images of Al/PVDF MIC films*

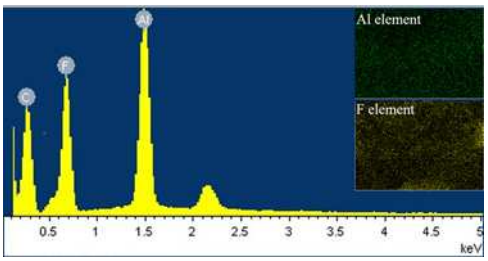

Fig. 3 *EDS images of Al/PVDF MIC films*

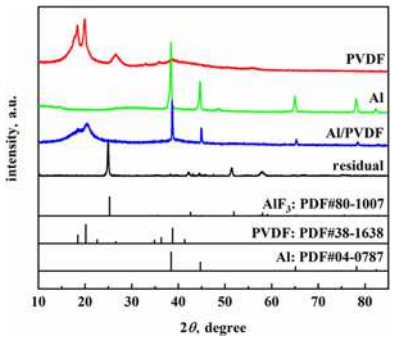

Fig. 4 *XRD patterns of Al, PVDF, Al/PVDF and reaction residue*

doi: 10.1049/mnl.2020.0238

(012), (113), (024) and (116) planes, respectively, confirm the dominant crystalline phase of α-AlF_3.

FTIR results (Fig. 5) show that three strong peaks of pure PVDF at 880, 1179 and 1402 cm^{-1} are due to the skeletal vibration of C–C bonds, stretching vibration of CF_2 groups and in-plane bending vibration of CH_2 groups, respectively. The characteristic peaks of α and β phases are all marked out [18, 26]. In addition, most characteristic peaks of PVDF could be found in the curve of Al/PVDF film, but the intensity of these peaks reduced greatly. These results show that heat treatment or preparation process has an obvious effect on the crystal form of PVDF.

The thermal stability and reactivity of Al/PVDF MIC films with different thickness were performed by TGA and DSC as shown in Fig. 6. The initial mass loss at around 101°C is due to the physical evaporation process of water (1.6–3.30% mass loss). As reported by McHale *et al.* [27], n-Al powder usually contains 3 wt% absorbed water. Starting from 360°C, Al/PVDF MIC film undergoes a main reaction step with an initial major mass reduction of about 35%. The remaining mass in 800°C is 60–70% for different thickness films. The results show that there is a reaction between the components of the composite. If only PVDF decomposition reaction occurs, the residual mass of the composite should be 48.78%, which means that most of the components are volatile products. According to Zulfiqar *et al.* [28], the main decomposition product of PVDF is HF, which highly agrees with our results. XRD result (Fig. 4) also shows that the dominant crystalline phase of residue is α-AlF_3, confirming the reaction [29].

Fig. 6*b* shows the DSC result, indicating that Al/PVDF MIC films have an endothermic peak at 150–175°C, which is caused by the melting of PVDF [30, 31]. For pure PVDF, there is only one main endothermic peak at about 450°C due to the thermal decomposition of PVDF [29]. Correspondingly, TGA results also show that the mass of PVDF declines rapidly between 400 and 500°C with a residual mass of 38.75%. The decomposition temperature of pure PVDF is delayed nearly 60°C compared with Al/PVDF MIC films, indicating the destabilisation of PVDF because of the addition of n-Al. This may be the result of interaction between the surface oxide layer of n-Al and released fluorine from PVDF, leading to the formation of AlF_3 that may catalyse the decomposition of PVDF [13]. For Al/PVDF MIC films, the reaction could be divided into two main exothermic processes. The first exothermic process corresponds to the reaction between the oxide layer on the surface of n-Al and the fluoride in the molten PVDF, also known as the PIR, leading to the fast decomposition of PVDF, which has been observed previously for the reaction of Al and PTFE [32]. AlF_3 may evaporate, so this does not prevent residual n-Al from reacting with PVDF. The second step is the reaction between core Al and PVDF decomposition products (or PVDF matrix), resulting in the subsequent two main exothermic peaks as shown in Fig. 6*b*. In addition, a small endothermic peak at 660°C from the melting of unreacted n-Al indicates that there is some remaining n-Al [33, 34].

To compare the relationship between reactive property and the thickness of the MIC films, we prepared three different thickness films (100, 200 and 300 μm) by solution casting method. The thickness of the film is measured by a micrometer caliper. Interestingly, Table 1 shows that dry film thickness is about one-tenth of that of wet film. It is well considered that the interfacial contact between fuel and oxidiser plays an important role in the thermal performance of MICs [35]. As shown in Fig. 6, heat output and mass loss increased greatly as the thickness of MIC films decreased. The maximum heat output of the main exothermic peak is 1032 J/g with film thickness of 100 μm. This may be explained as follows. Although the films have the same composition, the distance between fuel and oxidiser is reduced and the agglomeration phenomenon is effectively improved as the film thickness decreases.

DSC analysis with heating rates of 5, 10, 15 and 20 K/min in a nitrogen atmosphere was employed to evaluate the thermal degradation kinetics of Al/PVDF MIC films with thickness of 300 μm (Fig. 7). The apparent activation energy is determined from plotting $\ln(\beta/T_P^2)$ against $1/T_P$ by Kissinger method [36] and plotting $\ln(\beta/T_P^{1.8})$ against $1/T_P$ by Starink method [37]. Kissinger and Starink equations are shown in (3) and (4), respectively. The peak temperatures and apparent activation energies are shown in Table 2

$$\ln\frac{\beta}{T_P^2} = \ln\frac{AR}{E_a} - \frac{E_a}{RT_P} \tag{3}$$

$$\ln\frac{\beta}{T_P^{1.8}} = \text{Constant} - 1.0037\frac{E_a}{RT_P} \tag{4}$$

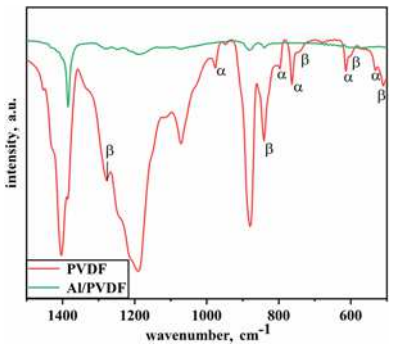

Fig. 5 *FTIR results of PVDF and Al/PVDF film*

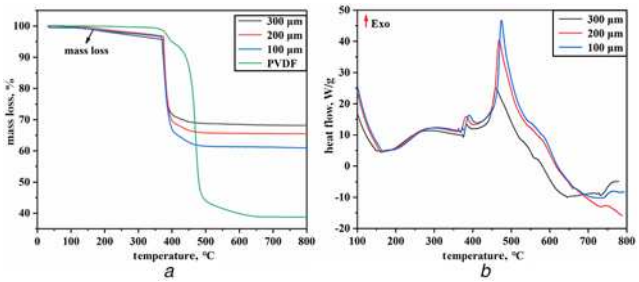

Fig. 6 *Thermal analysis of Al/PVDF MIC films with three thicknesses at heating rate of 10 K/min*
a TGA
b DSC

Table 1 Thicknesses of Al/PVDF films ($n = 5$)

thickness of wet films, μm	100	200	300
thickness of dry films, μm	12 ± 1	23 ± 1	32 ± 2

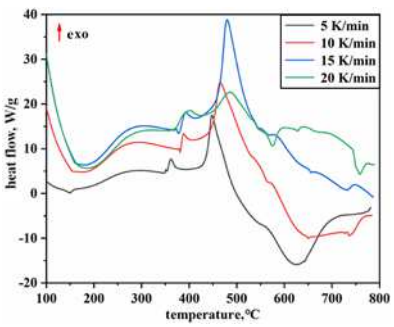

Fig. 7 *DSC results of Al/PVDF MIC films (300 μm) with different heating rates*

Table 2 Peak temperatures by DSC at different heating rates

	Peak temperature, K			
	5 K/min	10 K/min	15 K/min	20 K/min
Stage 1	613.64	630.62	641.73	644.96
Stage 2	644.99	660.56	664.93	674.37
Stage 3	721.21	738.56	753.06	758.61

Table 3 Apparent activation energies calculated by different methods

	Apparent activation energy, kJ/mol		Average value, kJ/mol
	Kissinger	Starink	
Stage 1	128.57 ($R^2 = 0.98583$)	129.14 ($R^2 = 0.98605$)	128.86
Stage 2	164.44 ($R^2 = 0.97796$)	164.93 ($R^2 = 0.97810$)	164.69
Stage 3	150.38 ($R^2 = 0.99210$)	155.93 ($R^2 = 0.99242$)	153.16

where β is heating rate, A is pre-exponential factor, R is gas constant, E_a is apparent activation energy and T_P is peak temperature.

Fig. 7 demonstrates that the reaction of Al/PVDF MIC films could be divided into three stages (Table 3). For the first stage, a small mass loss with the activation energy of 128.86 kJ/mol is attributed to the PIR reaction. The subsequent two stages with activation energy of 164.69 and 153.16 kJ/mol corresponding to the main mass loss are due to the reaction between core Al and PVDF decomposition products (or PVDF matrix). The results show that the activation energy calculated by the two methods ($R^2 > 0.975$) is very close to each other, indicating that the calculation results are highly reliable. The activation energy of Al/PVDF MIC films is lower than the results of Huang *et al.* [29] (182.9, 163.6, 176.0 kJ/mol, respectively, by powder mixing method), which means that Al/PVDF MIC films prepared by solution casting are prone to reaction.

4. Conclusion: Al/PVDF MIC films were successfully prepared by a solution casting method, and the thermal reaction properties of them were investigated. PVDF reacts with Al_2O_3 shell and oxidises the aluminium core of n-Al during the heating process, resulting in the formation of α-AlF_3. The addition of n-Al promotes the decomposition of PVDF, despite this occurs well below the temperature of aluminium melting. The heat output and mass loss increase as the thickness of Al/PVDF films decreases. The maximum heat release of the main exothermic peak is 1032 J/g (100 μm). The reaction kinetics process could be divided into three stages with apparent activation energy calculated by Kissinger and Starink methods of 128.86, 164.69 and 153.16 kJ/mol, respectively. In addition, this preparation method, fully compatible with micro-electro-mechanical system technology, is a promising way to prepare micrometre thick MIC films.

5. Acknowledgment: This paper is supported by the project of State Key Laboratory of Explosion Science and Technology (Beijing Institute of Technology, China) (no.YBKT19-04).

6 References

[1] Aumann C.E., Skofronick G.L., Martin J.A.: 'Oxidation behavior of aluminum nanopowders', *J. Vac. Sci. Technol., B*, 1995, **13**, (3), pp. 1178–1183
[2] Clayton N.A., Kappagantula K.S., Pantoya M.L., *ET AL.*: 'Fabrication, characterization, and energetic properties of metallized fibers', *ACS Appl. Mater. Interfaces*, 2014, **6**, (9), pp. 6049–6053
[3] Yan S., Jian G., Zachariah M.R.: 'Electrospun nanofiber-based thermite textiles and their reactive properties', *ACS Appl. Mater. Interfaces*, 2012, **4**, (12), pp. 6432–6435
[4] Sanders V.E., Asay B., Foley T.J., *ET AL.*: 'Reaction propagation of four nanoscale energetic composites (Al/MoO_3, Al/WO_3, Al/CuO, and Bi_2O_3)', *J. Propul. Power*, 2007, **23**, (4), pp. 707–714
[5] Maleki A.: 'One-pot three-component synthesis of pyrido[20,10:2,3] imidazo[4,5-c]isoquinolines using Fe_3O_4@SiO_2–OSO_3H as an efficient heterogeneous nanocatalyst', *RSC Adv.*, 2014, **4**, pp. 64169–64173
[6] Maleki A.: 'One-pot multicomponent synthesis of diazepine derivatives using terminal alkynes in the presence of silica-supported superparamagnetic iron oxide nanoparticles', *Tetrahedron Lett.*, 2013, **54**, pp. 2055–2059
[7] Maleki A.: 'Fe_3o_4/SiO_2 nanoparticles: an efficient and magnetically recoverable nanocatalyst for the one-pot multicomponent synthesis of diazepines', *Tetrahedron*, 2012, **68**, (38), pp. 7827–7833
[8] Maleki A., Hajizadeh Z., Sharifi V., *ET AL.*: 'A green, porous and eco-friendly magnetic geopolymer adsorbent for heavy metals removal from aqueous solutions', *J. Cleaner Prod.*, 2019, **2015**, pp. 1233–1245
[9] Sullivan K.T., Young G., Zachariah M.R.: 'Enhanced reactivity of nano-B/Al/CuO MIC's', *Combust. Flame*, 2009, **156**, (2), pp. 302–309
[10] Wang Y.J., Li Z.X., Yu H.Y, *ET AL.*: 'Reaction mechanism of metastable intermolecular composite', *Prog. Chem.*, 2016, **28**, (11), pp. 1689–1704
[11] He W., Liu P.J., Gong F.Y.: 'Tuning the reactivity of metastable intermixed composite n-Al/PTFE by polydopamine interfacial control', *ACS Appl. Mater. Interfaces*, 2018, **10**, (38), pp. 32849–32858
[12] Delisio J.B., Hu X.L., Wu T., *ET AL.*: 'Probing the reaction mechanism of aluminum/poly(vinylidene fluoride) composites', *J. Phys. Chem. B*, 2016, **120**, (24), pp. 5534–5542
[13] Mccollum J., Morey A.M., Iacono S.T.: 'Morphological and combustion study of interface effects in aluminum-poly(vinylidene fluoride) composites', *Mater. Des.*, 2017, **134**, pp. 64–70
[14] Wang Y., Travas-Sejdic J., Steiner R.: 'Polymer gel electrolyte supported with microporous polyolefin membranes for lithium ion polymer battery', *Solid State Ion.*, 2002, **148**, (3-4), p. 443–449
[15] He W., Li Z.H., Chen S.W.: 'Energetic metastable n-Al@PVDF/EMOF composite nanofibers with improved combustion performances', *Chem. Eng. J.*, 2018, **383**, pp. 123146–123155
[16] Guo L., Wang Y.J., He P.F., *ET AL.*: 'Spin coating preparation and thermal properties of metastable Al/PVDF energetic film with graphene', *Mater. Res. Express*, 2019, **6**, (8), pp. 086415–086424
[17] Wang H.Y., DeLisio J.B., Holdren S.: 'Mesoporous silica spheres incorporated aluminum/poly(vinylidene fluoride) for enhanced burning propellants', *Adv. Eng. Mater.*, 2017, **20**, (2), pp. 1700547–1700553
[18] Ke X., Guo S.F., Zhang G.S., *ET AL.*: 'Safe preparation, energetic performance and reaction mechanism of corrosion-resistant Al/PVDF nanocomposite films', *J. Phys. Chem. A*, 2018, **6**, (36), pp. 17713–17723
[19] Meeks K., Pantoya M.L., Apblett C.: 'Deposition and characterization of energetic thin films', *Combust. Flame*, 2014, **161**, pp. 1117–1124
[20] Wang H.Y., Rehwoldt M., Kline D.J., *ET AL.*: 'Comparison study of the ignition and combustion characteristics of directly-written Al/PVDF, Al/Viton and Al/THV composites', *Combust. Flame*, 2019, **201**, pp. 181–186
[21] Xu H.M., Li R., Shen J.P., *ET AL.*: 'Preparation and characterization of nanofibrous CuO/Al metastable intermolecular composite films', *IET Micro Nano Lett.*, 2012, **7**, (12), pp. 1251–1255
[22] Wang C.L., Shaw L.L.: 'On synthesis of Fe_2SiO_4/SiO_2 and Fe_2O_3/SiO_2 composites through sol–gel and solid-state reactions', *J. Sol-Gel Sci. Technol.*, 2014, **72**, (3), pp. 602–614
[23] Zhou X., Xu D.G., Lu J., *ET AL.*: 'Cuo/Mg/fluorocarbon sandwich-structure superhydrophobic nanoenergetic composite with anti-humidity property', *Chem. Eng. J.*, 2015, **266**, pp. 163–170
[24] Kwon Y.S., Gromov A.A., Strokova J.I.: 'Passivation of the surface of aluminum nanopowders by protective coatings of the different chemical origin', *Appl. Surf. Sci.*, 2007, **253**, (12), pp. 5558–5564
[25] Zheng L.B., Wu Z.J., Zhang Y., *ET AL.*: 'Effect of non-solvent additives on the morphology, pore structure, and direct contact membrane distillation performance of PVDF-CTFE hydrophobic membranes', *Am. J. Environ. Sci.*, 2016, **45**, pp. 28–39
[26] He F.A., Lin K., Shi D.L., *ET AL.*: 'Preparation of organosilicate/PVDF composites with enhanced piezoelectricity and pyroelectricity by stretching', *Compos. Sci. Technol.*, 2016, **137**, pp. 138–147

doi: 10.1049/mnl.2020.0238

[27] McHale H.J., Auroux A., Perrotta A.J., *ET AL.*: 'Surface energies and thermodynamic phase stability in nanocrystalline aluminas', *Science*, 1997, **277**, (5327), pp. 788–791
[28] Zulfiqar S., Zulfiqar M., Rizvi M., *ET AL.*: 'Study of the thermal degradation of polychlorotrifluoroethylene, poly(vinylidene fluoride) and copolymers of chlorotrifluoroethylene and vinylidene fluoride', *Polym. Degrad. Stab.*, 1994, **43**, (3), pp. 423–430
[29] Huang C., Yang H.T., Li Y.C., *ET AL.*: 'Characterization of aluminum/poly(vinylidene fluoride) by thermogravimetric analysis, differential scanning calorimetry, and mass spectrometry', *Anal. Lett.*, 2015, **48**, (13), pp. 2011–2021
[30] Mendes S., Carlos C., Vitor S., *ET AL.*: 'Thermal degradation of Pb $(Zr_{0.53}Ti_{0.47})O_3$/poly(vinylidene fluoride) composites as a function of ceramic grain size and concentration', *J. Therm. Anal. Calorim.*, 2013, **114**, pp. 757–763
[31] Botelho G., Lanceros M.S., GonAlves A.M., *ET AL.*: 'Relationship between processing conditions, defects and thermal degradation of poly(vinylidene fluoride) in the β-phase', *J. Non-Cryst. Solids*, 2008, **354**, (1), pp. 72–78
[32] Pantoya M.L., Dean S.W.: 'The influence of alumina passivation on nano-Al/Teflon', *Thermochim. Acta*, 2009, **493**, (1-2), pp. 109–110
[33] Dreizin E.L.: 'Metal-based reactive nanomaterial', *Prog. Energy Combust. Sci.*, 2009, **35**, (2), pp. 141–167
[34] Trunov M.A., Umbrajkar S.M., Schoenitz M., *ET AL.*: 'Oxidation and melting of aluminum nanopowders', *J. Phys. Chem. B*, 2006, **110**, (26), pp. 13094–13099
[35] Sullivan K.T., Piekiel N.W., Wu C., *ET AL.*: 'Reactive sintering: an important component in the combustion of nanocomposite thermites', *Combust. Flame*, 2012, **159**, (1), pp. 2–15
[36] Kissinger H.E.: 'Reaction kinetics in differential thermal analysis', *Anal. Chem.*, 1957, **29**, (11), pp. 1702–1706
[37] Starink M.J.: 'On the meaning of the impingement parameter in kinetic equations for nucleation and growth reactions', *J. Mater. Sci.*, 2001, **36**, (18), pp. 4433–4441